

Azimuthal anisotropies for Au+Au collisions in the parton-hadron transient energy range

V. P. Konchakovski,^{1,2} E. L. Bratkovskaya,^{3,4} W. Cassing,¹ V. D. Toneev,^{4,5} S. A. Voloshin,⁶ and V. Voronyuk^{2,4,5}

¹*Institute for Theoretical Physics, University of Giessen, Giessen, Germany*

²*Bogolyubov Institute for Theoretical Physics, Kiev, Ukraine*

³*Institute for Theoretical Physics, University of Frankfurt, Frankfurt, Germany*

⁴*Frankfurt Institute for Advanced Studies, Frankfurt, Germany*

⁵*Joint Institute for Nuclear Research, Dubna, Russia*

⁶*Wayne State University, Detroit, Michigan, USA*

The azimuthal anisotropies of the collective transverse flow of charged hadrons are investigated in a wide range of heavy-ion collision energies within the microscopic parton-hadron-string dynamics (PHSD) transport approach, which incorporates explicit partonic degrees of freedom in terms of strongly interacting quasiparticles (quarks and gluons) in line with an equation of state from lattice QCD as well as the dynamical hadronization and hadronic collision dynamics in the final reaction phase. The experimentally observed increase of the elliptic flow v_2 of charged hadrons with collision energy is successfully described in terms of the PHSD approach. The PHSD scaling properties of various collective observables are confronted with experimental data as well as with hydrodynamic predictions. The analysis of higher-order harmonics v_3 and v_4 in the azimuthal angular distribution shows a similar tendency of growing deviations between partonic and purely hadronic models with increasing collision energy. This demonstrates that the excitation functions of azimuthal anisotropies reflect the increasing role of quark-gluon degrees of freedom in the early phase of relativistic heavy-ion collisions. Furthermore, the specific variation of the ratio $v_4/(v_2)^2$ with respect to bombarding energy, centrality, and transverse momentum is found to provide valuable information on the underlying dynamics.

PACS numbers: 25.75.-q, 25.75.Ag

I. INTRODUCTION

The discovery of large azimuthal anisotropic flow at the Relativistic Heavy Ion Collider (RHIC) provides conclusive evidence for the creation of dense partonic matter in ultra relativistic nucleus-nucleus collisions. With sufficiently strong parton interactions, the medium in the collision zone can be expected to achieve local equilibrium and exhibit approximately hydrodynamic flow [1–3]. The momentum anisotropy is generated due to pressure gradients of the initial “almond-shaped” collision zone produced in noncentral collisions [1, 2]. The azimuthal pressure gradient extinguishes itself soon after the start of the hydrodynamic evolution, so the final flow is insensitive to later stages of the fireball evolution. The pressure gradients have to be large enough to translate an early asymmetry in density of the initial state to a final-state momentum-space anisotropy. In these collisions a new state of strongly interacting matter is created, being characterized by a very low shear viscosity η to entropy density s ratio, η/s , close to a nearly perfect fluid [4–6]. Lattice QCD (lQCD) calculations [7–9] indicate that a crossover region between hadron and quark-gluon matter should have been reached in these experiments.

An experimental manifestation of this collective flow is the anisotropic emission of charged particles in the plane transverse to the beam direction. This anisotropy is described by the different flow parameters defined as the proper Fourier coefficients v_n of the particle distributions in azimuthal angle ψ with respect to the reaction

plane angle Ψ_{RP} . At the highest RHIC collision energy of $\sqrt{s_{NN}} = 200$ GeV, differential elliptic flow measurements $v_2(p_T)$ have been reported for a broad range of centralities or number of participants N_{part} . For N_{part} estimates, the geometric fluctuations associated with the positions of the nucleons in the collision zone serve as the underlying origin of the initial eccentricity fluctuations. These data are found to be in accord with model calculations that an essentially locally equilibrated quark-gluon plasma (QGP) has little or no viscosity [2, 10–12]. Collective flow continues to play a central role in characterizing the transport properties of the strongly interacting matter produced in heavy-ion collisions at RHIC. Particle anisotropy measurements are considered as key observables for a reliable extraction of transport coefficients.

A quark-number scaling of the elliptic-flow data is observed for a broad range of particle species, collision centralities, and transverse kinetic energy, which is interpreted as being due to the development of substantial collectivity in the partonic phase [13]. Small violations of the scaling of $v_2(N_{part})$ with the initial eccentricity of the collision zone ϵ_2 suggest a strongly coupled low-viscosity plasma $\eta/s \sim (1-2)/(4\pi)$ in energetic Au+Au collisions [13–15]. The initial eccentricity of the collision zone (and its associated fluctuations) has proven to be an essential ingredient for these extractions. Nevertheless, the degree to which the QGP is thermalized is still being debated [16].

It was shown before that higher-order anisotropy harmonics, in particular v_4 , may provide a more sensitive

constraint on the magnitude of η/s and the freeze-out dynamics, and the ratio $v_4/(v_2)^2$ might indicate whether a full local equilibrium is achieved in the QGP [17]. The role of fluctuations and so-called nonflow correlations are important for such measurements. It is well established that initial eccentricity fluctuations significantly influence the magnitudes of $v_{2,4}$ [18]. However, the precise role of nonflow correlations, which lead to a systematic error in the determination of $v_{2,4}$, is less clear. Recently, significant attention has been given to the study of the influence of initial geometry fluctuations on higher order eccentricities $\epsilon_n (n \geq 3)$ for a better understanding of how such fluctuations manifest themselves in the harmonic flow correlations characterized by v_n . Even more, it was proposed that the analysis of v_n^2 for all values of n can be considered as an analogous measurement to the power spectrum extracted from the cosmic microwave background Radiation providing a possibility to observe superhorizon fluctuations [19].

More recently, the importance of the triangular flow v_3 , which originates from fluctuations in the initial collision geometry, has been pointed out [20–22]. The participant triangularity characterizes the triangular anisotropy of the initial nuclear overlap geometry. It arises from event-by-event fluctuations in the participant-nucleon collision space-time points and corresponds to a large third Fourier component in the two-particle azimuthal correlations at large pseudo rapidity separation $\Delta\eta$. This fact suggests a significant contribution of the triangular flow to the ridge phenomenon and broad away-side structures observed in the RHIC data [23]. The ridge might be related to flux-tube-like structures in the initial state as argued in Ref. [24] or successive coherent gluon radiation as suggested in Ref. [25].

A large number of anisotropic flow measurements have been performed by many experimental groups at SIS (Schwerionensynchrotron), AGS (Alternating Gradient Synchrotron), SPS (Super Proton Synchrotron), and RHIC (Relativistic Heavy Ion Collider) energies over the last twenty years. Very recently, the azimuthal asymmetry has been measured also at the LHC (Large Hadron Collider) [26]. However, the fact that these data have not been obtained under the same experimental conditions as at RHIC experiments, does not directly allow for a detailed and meaningful comparison in most cases. The experimental differences include different centrality selection, different transverse momentum acceptance, different particle species, different rapidity coverage, and different methods for flow analysis as pointed out in Ref. [27].

The Beam Energy Scan (BES) program proposed at RHIC [28] covers the energy interval from $\sqrt{s_{NN}} = 200$ GeV, where partonic degrees of freedom play a decisive role, down to the AGS energy of $\sqrt{s_{NN}} \approx 5$ GeV, where most experimental data may be described successfully in terms of hadronic degrees of freedom, only. Lowering the RHIC collision energy and studying the energy dependence of anisotropic flow allows us to search for the

possible onset of the transition to a phase with partonic degrees of freedom at an early stage of the collision, as well as possibly to identify the location of the critical end point that terminates the crossover transition at small quark-chemical potential to a first-order phase transition at higher quark-chemical potential [13, 29].

This work aims to study excitation functions for different harmonics of the charged-particle anisotropy in the azimuthal angle at midrapidity in a wide transient energy range, *i.e.*, from the AGS to the top RHIC energy. The first attempts to explain the preliminary STAR data with respect to the observed increase of the elliptic flow v_2 with the collision energy have failed, since the traditional available models did not allow clarification of the role of the partonic phase [30]. In this paper, as an extension of our recent study in Ref. [31], we investigate the energy behavior of different flow coefficients, their scaling properties and differential distributions. Our analysis of the STAR/PHENIX RHIC data – based on recent results of the BES program – will be performed within the parton-hadron-string dynamics (PHSD) transport model [32] that includes explicit partonic degrees of freedom as well as a dynamical hadronization scheme for the transition from partonic to hadronic degrees of freedom and vice versa.

The paper is organized as follows: In Section II we will briefly recall the main ingredients of the PHSD approach as well as the performance of PHSD for relativistic heavy-ion collisions from the lower SPS to the top RHIC energies. Section III is devoted to the actual results from PHSD for the excitation function of the elliptic flow v_2 in comparison to the hadron-string dynamics (HSD) approach and other related models, as well as to the available data from the STAR and PHENIX Collaborations. We also provide results from the PHSD and HSD models for the excitation functions of v_3 and v_4 in view of the Beam Energy Scan (BES) program at RHIC in order to identify partonic contributions. Scaling properties of experimental data, in particular the universal and longitudinal scaling relations found empirically, are elaborated here and compared to a hydrodynamic description. To be more specific, we will also present the calculated results for the p_T dependence of elliptic flow at midrapidity for minimum bias collisions of Au+Au for $\sqrt{s_{NN}}$ from 5 to 200 GeV. Furthermore, the centrality dependence of v_2 , v_3 , and v_4 will be addressed at the top RHIC energy. Section IV provides the conclusions of our present study and indicates the open problems.

II. THE PHSD MODEL

The dynamics of partons, hadrons and strings in relativistic nucleus-nucleus collisions is analyzed within the novel parton-hadron-string dynamics (PHSD) approach [32, 33]. In this transport approach the partonic dynamics is based on the dynamical quasiparticle model (DQPM) [34, 35], which describes QCD properties in

terms of single-particle Green's functions [in the sense of a two-particle irreducible (2PI) approach]. In Ref. [33] the actual (essentially three) DQPM parameters for the temperature-dependent effective coupling have been fitted to the recent lattice QCD results of Ref. [9]. The latter lead to a critical temperature $T_c \approx 160$ MeV, which corresponds to a critical energy density of $\varepsilon_c \approx 0.5$ GeV/fm³. In PHSD the parton spectral functions ρ_j ($j = q, \bar{q}, g$) are no longer δ -functions in the invariant mass squared (as in conventional cascade or transport models), but are taken as

$$\rho_j(\omega, \mathbf{p}) = \frac{\gamma_j}{E_j} \left(\frac{1}{(\omega - E_j)^2 + \gamma_j^2} - \frac{1}{(\omega + E_j)^2 + \gamma_j^2} \right) \quad (1)$$

separately for quarks/antiquarks and gluons ($j = q, \bar{q}, g$). With the convention $E^2(\mathbf{p}^2) = \mathbf{p}^2 + M_j^2 - \gamma_j^2$, the parameters M_j^2 and γ_j are directly related to the real and imaginary parts of the retarded self-energy, *e.g.*, $\Pi_j = M_j^2 - 2i\gamma_j\omega$. The spectral function (1) is anti-symmetric in ω and is normalized as

$$\int_{-\infty}^{\infty} \frac{d\omega}{2\pi} \omega \rho_j(\omega, \mathbf{p}) = \int_0^{\infty} \frac{d\omega}{2\pi} 2\omega \rho_j(\omega, \mathbf{p}) = 1. \quad (2)$$

The actual parameters in Eq. (1), *i.e.*, the gluon mass M_g and width γ_g – employed as input in the PHSD calculations – as well as the quark mass M_q and width γ_q , are depicted in Fig. 1 of Ref. [33] as a function of the scaled temperature T/T_c . As mentioned above, these values for the masses and widths have been fixed by fitting the lattice QCD results from Ref. [9] in thermodynamic equilibrium. We recall that the DQPM allows extraction of a potential energy density V_p from the space-like part of the energy-momentum tensor, which can be tabulated, *e.g.*, as a function of the scalar parton density ρ_s . Derivatives of V_p with respect to ρ_s then define a scalar mean-field potential $U_s(\rho_s)$, which enters the equation of motion for the dynamical partonic quasiparticles. As one can see from Fig. 1, the scalar potential is rather large and non-linearly increases with ρ_s . This implies that the repulsive force due to $U_s(\rho_s)$ will change in a nonmonotonous way with the scalar density. The vector mean-field potential is not negligible too, especially at high ρ_s , and induces a Lorentz force for the partons. Note that the vector mean-field potential vanishes with decreasing scalar density whereas the scalar mean-field potential approaches a constant value for $\rho_s \rightarrow 0$.

Furthermore, a two-body interaction strength can be extracted from the DQPM as well from the quasiparticle width in line with Ref. [6] (*cf.* Refs. [32, 33] for details). The transition from partonic to hadronic degrees of freedom (and vice versa) is described by covariant transition rates for the fusion of quark-antiquark pairs or three quarks (antiquarks), respectively, obeying flavor current-conservation, color neutrality, as well as energy-momentum conservation. Since the dynamical quarks and antiquarks become very massive close to

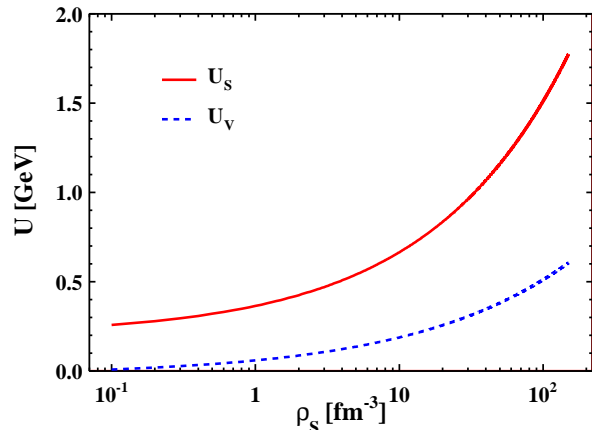


FIG. 1: (Color online) The scalar and vector mean-field potentials in the present PHSD model as a function of the scalar density ρ_s of partons.

the phase transition, the formed resonant “pre-hadronic” color-dipole states ($q\bar{q}$ or qqq) are of high invariant mass too, and sequentially decay to the ground-state meson and baryon octets, increasing the total entropy.

On the hadronic side PHSD includes explicitly the baryon octet and decouplet, the 0^- - and 1^- -meson nonets, as well as selected higher resonances as in the hadron-string dynamics (HSD) approach [36, 37]. Hadrons of higher masses (>1.5 GeV in the case of baryons and >1.3 GeV in the case of mesons) are treated as “strings” (color dipoles) that decay to the known (low-mass) hadrons according to the JETSET algorithm [38]. We discard an explicit recapitulation of the string formation and decay and refer the reader to the original work [38]. Note that PHSD and HSD (without explicit partonic degrees of freedom) merge at low energy density, in particular below the critical energy density $\varepsilon_c \approx 0.5$ GeV/fm³.

The PHSD approach has been applied to nucleus-nucleus collisions from $\sqrt{s_{NN}} \sim 5$ to 200 GeV in Refs. [32, 33] in order to explore the space-time regions of “partonic matter”. It was found that even central collisions at the top SPS energy of $\sqrt{s_{NN}} = 17.3$ GeV show a large fraction of nonpartonic, *i.e.*, hadronic or string-like matter, which can be viewed as a hadronic corona. This finding implies that neither hadronic nor only partonic “models” can be employed to extract physical conclusions in comparing model results with data. In addition, we have found that the partonic phase has a low impact on rapidity distributions of hadrons but a sizable influence on the transverse mass distribution of final kaons due to the repulsive partonic mean fields [32]. It has been, furthermore, demonstrated in Ref. [33] that at $\sqrt{s_{NN}} = 200$ GeV the PHSD model gives a reasonable reproduction of hadron rapidity distributions and transverse mass spectra, and also a fair description of the elliptic flow of charged hadrons as a function of the centrality of the

reaction and the transverse momentum p_T .

Furthermore, an approximate quark-number scaling of the elliptic flow v_2 of identified hadrons is observed in the PHSD results at top RHIC energies too. As indicated above, PHSD merges to HSD in the lower (transient) energy regime. Both approaches are well in line with experimental data in the lower SPS energy regime as shown in Ref. [32]. All these previous findings provide promising perspectives to use PHSD in the whole range from about $\sqrt{s_{NN}} = 5$ to 200 GeV.

III. RESULTS FOR COLLECTIVE FLOWS

A. Elliptic flow

The largest component, known as elliptic flow v_2 , is one of the early observations at RHIC [39]. More recently, it was noticed that fluctuations in the initial geometry are very important [20]. The elliptic flow coefficient is a widely used quantity characterizing the azimuthal anisotropy of emitted particles,

$$v_2 = \langle \cos(2\psi - 2\Psi_{RP}) \rangle = \left\langle \frac{p_x^2 - p_y^2}{p_x^2 + p_y^2} \right\rangle, \quad (3)$$

where Ψ_{RP} is the azimuth of the reaction plane, p_x and p_y are the x and y component of the particle momenta, and the brackets denote averaging over particles and events. This coefficient can be considered as a function of centrality, pseudorapidity η , and/or transverse momentum p_T . We note that the reaction plane in PHSD is given by the $x - z$ plane with the z axis in the beam direction. The reaction plane is defined as a plane containing the beam axes and the impact parameter vector.

We recall that at high bombarding energies the longitudinal size of the Lorentz contracted nuclei becomes negligible compared to its transverse size. The forward shadowing effect then goes away and the elliptic flow fully develops in-plane, leading to a positive value of the average flow v_2 since no shadowing from spectators takes place. In Fig. 2 the experimental v_2 data compilation for the transient energy range is compared to the results from HSD calculations and further available model results as included in Ref. [30]. The centrality selection is the same for the data and the various models.

In order to interpret the results in Fig. 2 we have to recall the various ingredients of the models employed for comparison. The UrQMD (ultrarelativistic quantum molecular dynamics) model is a microscopic transport theory based on the relativistic Boltzmann equation [40]. It allows for the on-shell propagation of all hadrons along classical trajectories in combination with stochastic binary scattering, color string formation, and resonance decay. The model incorporates baryon-baryon, meson-baryon, and meson-meson interactions based on experimental data (when possible). This Boltzmann-like hadronic transport model has been employed for proton-nucleus and nucleus-nucleus collisions from AGS to RHIC

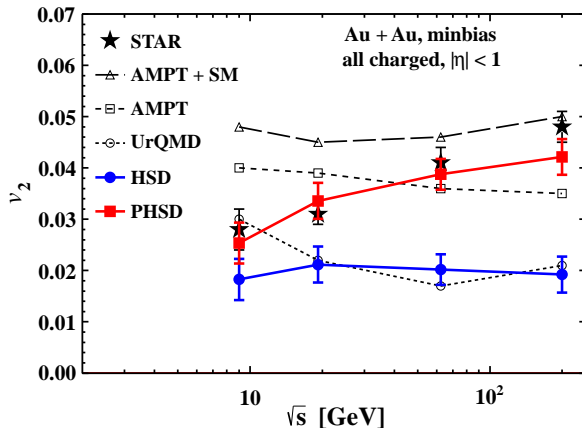


FIG. 2: (Color online) The average elliptic flow v_2 of charged particles at midrapidity for minimum bias collisions at $\sqrt{s_{NN}} = 9.2, 19.6, 62.4$ and 200 GeV (given by stars) is taken from the data compilation of Ref. [30]. The corresponding results from different models are compared to the data and explained in more detail in the text.

energies [40]. The comparison of the data on v_2 to those from the UrQMD model will thus essentially provide information on the contribution from the hadronic phase. As seen in Fig. 2, being in agreement with data at the lowest energy $\sqrt{s_{NN}} = 9.2$ GeV, the UrQMD model results then either remain approximately constant or decrease slightly with increasing $\sqrt{s_{NN}}$; UrQMD thus does not reproduce the rise of v_2 with the collision energy as seen experimentally.

The HSD model [37, 41] is also a hadron-string model including formally the same processes as UrQMD. However, being based on the off-shell generalized transport equation [42] followed from Kadanoff-Baym approach, the quasiparticles in the HSD model take into account in-medium modifications of their properties in the nuclear environment, which is rather essential for many observables and in particular for dileptons. Detailed comparisons between HSD and UrQMD for central Au + Au (Pb + Pb) collisions have been reported in Refs. [43, 44] from AGS to top SPS energies with respect to a large experimental data set. Indeed, both hadronic approaches yield similar results on the level of 20%-30%, which is also the maximum deviation from the data sets. Accordingly, the HSD model also predicts an approximately energy-independent flow v_2 in quite close agreement with the UrQMD results. We may thus conclude that the rise of v_2 with bombarding energy is not due to hadronic interactions and models with partonic degrees of freedom have to be addressed.

The AMPT (a multi phase transport) model [45] uses initial conditions of a perturbative QCD (pQCD) inspired model, which produces multiple minijet partons according to the number of binary initial nucleon-nucleon collisions. These (massless) minijet partons undergo

scattering (without potentials) before they are allowed to fragment into hadrons. The string melting (SM) version of the AMPT model (labeled in Fig. 2 as AMPT-SM) is based on the idea that the existence of strings (or hadrons) is impossible for energy densities beyond a critical value of $\varepsilon \sim 1 \text{ GeV}/\text{fm}^3$. Hence they need to melt the strings to (massless) partons. This is done by converting the mesons to a quark and antiquark pair, baryons to three quarks, *etc.*, fulfilling energy-momentum conservation. The subsequent scatterings of the quarks are based on a parton cascade with (adjustable) effective cross sections that are significantly larger than those from pQCD [45]. Once the partonic interactions terminate, the partons hadronize through the mechanism of parton coalescence.

We find from Fig. 2 that the interactions between the minijet partons in the AMPT model indeed increase the elliptic flow significantly as compared to the hadronic models UrQMD and HSD. An additional inclusion of interactions between partons in the AMPT-SM model gives rise to another 20% of v_2 , bringing it into agreement (for AMPT-SM) with the data at the maximal collision energy. So, both versions of the AMPT model indicate the importance of partonic contributions to the observed elliptic flow v_2 but do not reproduce its growth with $\sqrt{s_{NN}}$. The authors address this result to the partonic equation of state (EoS) employed, which corresponds to a massless and noninteracting relativistic gas of particles. This EoS deviates severely from the results of lattice QCD calculations for temperatures below 2-3 T_c . Accordingly, the degrees of freedom are propagated without self-energies and a parton spectral function.

The PHSD approach incorporates the latter medium effects in line with a lQCD equation-of-state as discussed in Section II and also includes a dynamical hadronization scheme based on covariant transition rates. As has been shown in our previous study [31], the elliptic flow v_2 from PHSD (red solid lines in Figs. 2 and 3) agrees with the data from the STAR and PHENIX Collaborations and clearly shows an increase with bombarding energy. As was demonstrated in the thorough analysis of Ref. [27], the difference between STAR/PHENIX v_2 results is less than 2%-5% below $p_T \simeq 2.5 \text{ GeV}/c$. At higher transverse momentum, the STAR elliptic flow v_2 is systematically larger than the PHENIX v_2 and the ratio tends to grow with p_T , reaching the value of 20% at $p_T \simeq 5.5 \text{ GeV}/c$. The differences in v_2 at higher p_T might be attributed to non-flow effects due to di-jets, which are mostly suppressed by the rapidity gaps in the case of the PHENIX measurements. Anyhow, we do not consider such high transverse momenta.

Note that PHSD and AMPT-SM practically give the same elliptic flow at the top RHIC energy of $\sqrt{s_{NN}} = 200 \text{ GeV}$. However, PHSD is more elaborated and includes more realistic properties of dynamical quasiparticles, especially in the vicinity of the critical energy density.

An explanation for the increase in v_2 with collision en-

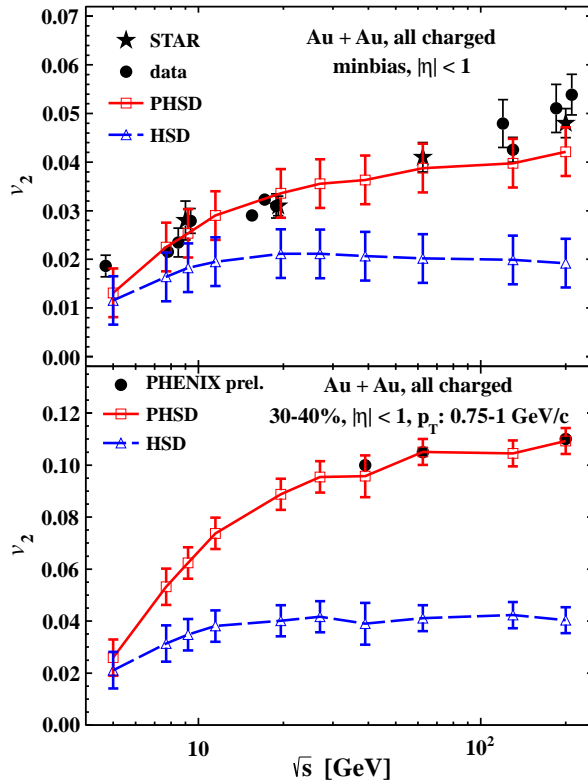


FIG. 3: (Color online) Average elliptic flow v_2 of charged particles at mid-pseudorapidity for two centrality selections calculated within the PHSD (solid curves) and HSD (dashed lines) models. The v_2 STAR data (stars) for minimal bias are the same as in Fig. 2 (stars); the preliminary PHENIX data [46] are plotted by filled circles and other data are taken from the compilation in Ref. [47].

ergy is provided in Fig. 4. Here we show the partonic fraction of the energy density with respect to the total energy where the energy densities are calculated at midrapidity. As discussed above, the main contribution to the elliptic flow is coming from an initial partonic stage at high \sqrt{s} . The fusion of partons to hadrons or, inversely, the melting of hadrons to partonic quasiparticles occurs when the local energy density is about $\varepsilon \approx 0.5 \text{ GeV}/\text{fm}^3$. As follows from Fig. 4, the parton fraction of the total energy goes down substantially with decreasing bombarding energy while the duration of the partonic phase is roughly the same. The maximal fraction reached is the same in central and peripheral collisions but the parton evolution time is shorter in peripheral collisions. One should recall again the important role of the repulsive mean-field potential for partons in the PHSD model (see Fig. 1) that leads to an increase of the flow v_2 with respect to HSD predictions (cf. also Ref. [48]). We point out in addition that the increase of v_2 in PHSD relative to HSD is also partly due to the higher interaction rates in the partonic medium because of a lower ratio of η/s for partonic degrees of freedom at energy densities above the criti-

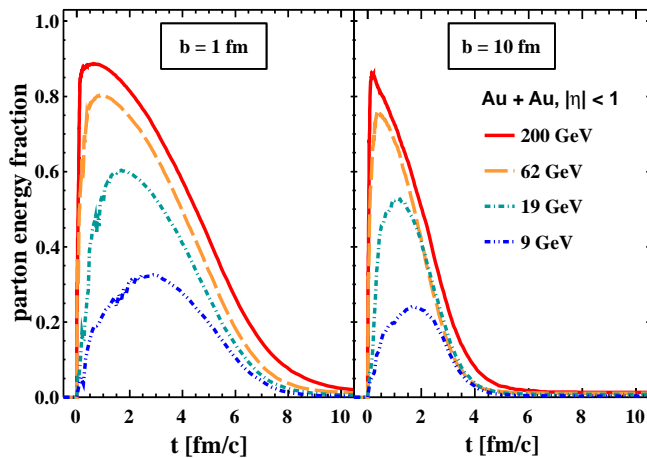


FIG. 4: (Color online) Evolution of the parton fraction of the total energy density at midrapidity for different collision energies at impact parameters $b = 1$ and 10 fm.

cal energy density than for hadronic media below the critical energy density [49, 50]. The relative increase in v_3 and v_4 in PHSD essentially is due to the higher partonic interaction rate and thus to a lower ratio η/s in the partonic medium, which is mandatory to convert initial spatial anisotropies to final anisotropies in momentum space [51].

B. Higher-order flow harmonics

Depending on the location of the participant nucleons in the nucleus at the time of the collision, the actual shape of the overlap area may vary: the orientation and eccentricity of the ellipse defined by the participants fluctuates from event to event. As seen from Fig. 5, due to fluctuations the overlap area in a single event can have, for example, a rotated triangular rather than an almond shape. Note, however, that by averaging over many events an almond shape is regained for the same impact parameter.

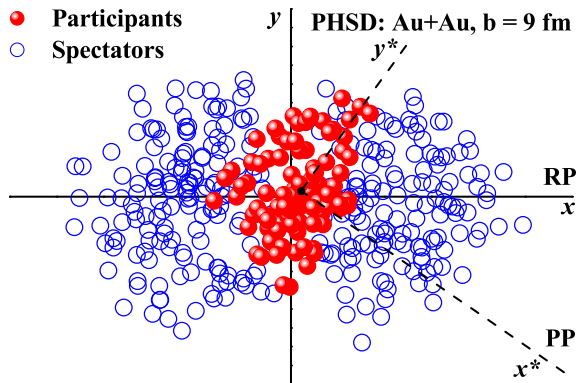


FIG. 5: (Color online) Projection of a single peripheral Au+Au (200 GeV) collision on the transverse plane. Spectator and participant nucleons are plotted by empty and filled circles, respectively. The participant plane transverse axes are marked by stars (x^* , y^*).

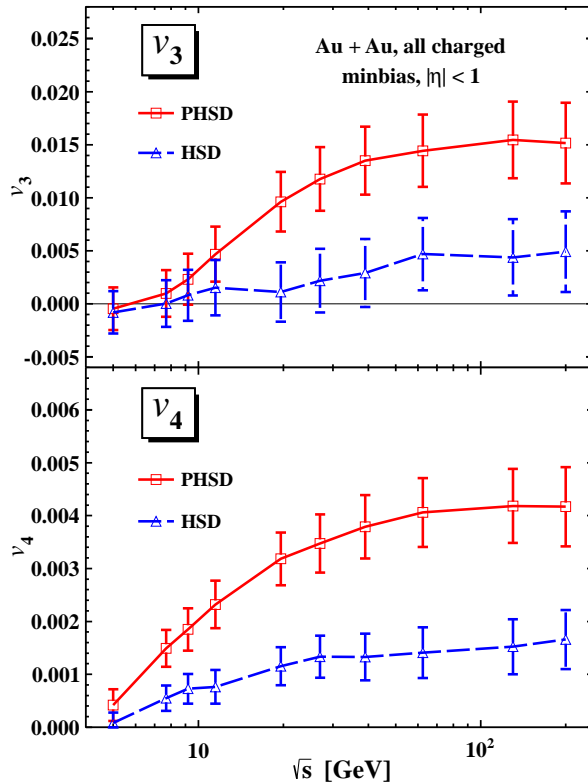


FIG. 6: (Color online) Average anisotropic flows v_3 and v_4 of charged particles at mid-pseudorapidity for minimum-bias Au + Au collisions calculated within the PHSD (solid line) and HSD (dashed line) models.

Recent studies suggest that fluctuations in the initial state geometry can generate higher-order flow components [10, 19, 20, 22]. The azimuthal momentum distribution of the emitted particles is commonly expressed in the form of Fourier series as

$$E \frac{d^3N}{d^3p} = \frac{d^2N}{2\pi p_T dp_T dy} \left(1 + \sum_{n=1}^{\infty} 2v_n(p_T) \cos[n(\psi - \Psi_n)] \right), \quad (4)$$

where v_n is the magnitude of the n th order harmonic term relative to the angle of the initial-state spatial plane of symmetry Ψ_n . The anisotropy in the azimuthal angle ψ is usually characterized by the even-order Fourier coefficients with the reaction plane $\Psi_n = \Psi_{RP}$: $v_n = \langle \exp(i n(\psi - \Psi_{RP})) \rangle$ ($n = 2, 4, \dots$), since for a smooth angular profile the odd harmonics vanish. For the odd components, say v_3 , one should take into account event-by-

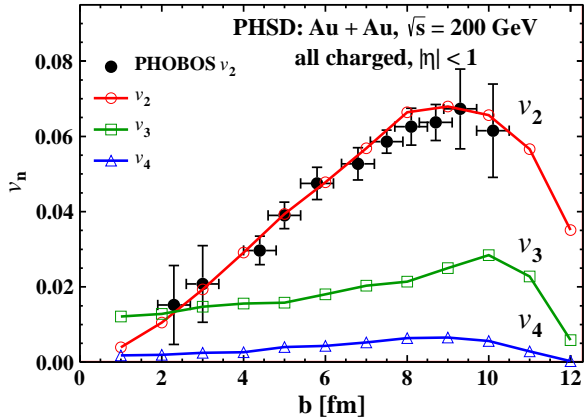


FIG. 7: (Color online) Impact parameter dependence of anisotropic flows of charged particles at mid-pseudorapidity for minimum-bias collisions of Au+Au at $\sqrt{s_{NN}} = 200$ GeV. Experimental points are from Ref. [55].

event fluctuations with respect to the participant plane $\Psi_n = \Psi_{PP}$. We calculate the v_3 coefficients with respect to Ψ_3 as $v_3\{\Psi_3\} = \langle \cos(3[\psi - \Psi_3]) \rangle / \text{Res}(\Psi_3)$. The event plane angle Ψ_3 and its resolution $\text{Res}(\Psi_3)$ are calculated as described in Ref. [52] via the two-sub-events method [53, 54].

In Fig. 6 we display the PHSD and HSD results for the anisotropic flows v_3 and v_4 of charged particles at mid-pseudorapidity for Au+Au collisions as a function of $\sqrt{s_{NN}}$. The pure hadronic model HSD gives $v_3 \approx 0$ for all energies. Accordingly, the results from PHSD (dashed red line) are systematically larger than from HSD (dashed blue line). Unfortunately, our statistics are not good enough to allow for more precise conclusions. The hexadecupole flow v_4 stays almost constant in the energy range $\sqrt{s_{NN}} \gtrsim 10$ GeV; at the same time the PHSD gives noticeably higher values than HSD, which we attribute to the higher interaction rate in the partonic phase, i.e., a lower ratio of η/s for the partonic degrees of freedom [49, 50].

Alongside with the integrated flow coefficients v_n the PHSD model reasonably describes their distribution over centrality or impact parameter b . A specific comparison at $\sqrt{s_{NN}} = 200$ GeV is shown in Fig. 7 for v_2 , v_3 , and v_4 . While v_2 increases strongly with b up to peripheral collisions, v_3 and v_4 are only weakly sensitive to the impact parameter. The triangular flow is always somewhat higher than the hexadecupole flow in the whole range of impact parameters b .

Recently, the triangular flow at $\sqrt{s_{NN}} = 200$ GeV has been recalculated in the updated AMPT model [56]. The values of model parameters for the Lund string fragmentation and the parton scattering cross section from the previous default version have been refitted to describe the charged multiplicity distribution, transverse momentum spectra, and elliptic flow for Au+Au collisions at

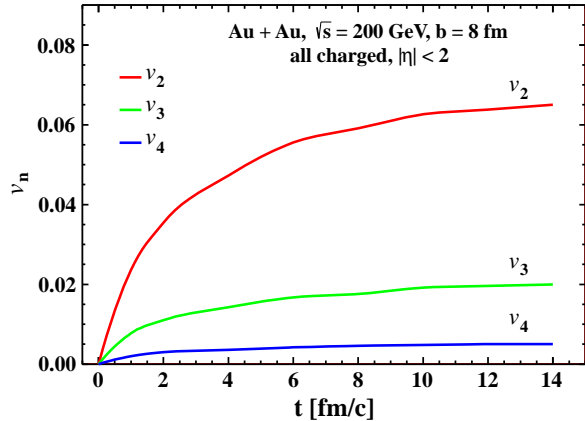


FIG. 8: (Color online) Time evolution of v_n for Au+Au collisions at $\sqrt{s_{NN}} = 200$ GeV with impact parameter $b = 8$ fm.

$\sqrt{s_{NN}} = 200$ GeV. In the novel AMPT version the parton scattering cross sections decrease from about 10 to 1.5 mb. As compared to the old AMPT result $v_3 \approx 0.4$, the new value $v_3 \approx 0.2$ is consistent with the PHSD results in Fig. 6. Note, that the magnitude of the PHSD triangular flow at $\sqrt{s_{NN}} = 200$ GeV is similar also to that from the (3 + 1)D viscous hydrodynamical model [57] with the specific viscosity $\eta/s = 0.08$. In our calculations the low transverse momentum particles with $p_T < 1$ GeV/c are dominating. Unfortunately, experimental data for this momentum range are not available.

Figure 8 shows the time evolution of flow coefficients v_2 , v_3 , and v_4 for a Au+Au collision at impact parameter $b=8$ fm. They reach their asymptotic values by the time of 6-8 fm/c after the beginning of the collision, which corresponds to the dominantly partonic phase (cf. Fig. 4). Thus, collective flows are formed in the early partonic stage of the collision.

Different harmonics can be related to each other. In particular, hydrodynamics predicts that $v_4 \propto (v_2)^2$ [58]. The simplest prediction that $v_4 = 0.5(v_2)^2$ is given for a boosted thermal freeze-out distribution of an ideal fluid, in Ref. [16]. In this work it was noted also that v_4 is largely generated by an intrinsic elliptic flow (at least at high p_T) rather than the fourth order moment of the fluid flow. This is a motivation for studying the ratio $v_4/(v_2)^2$ rather than v_4 alone. As is seen in Fig. 9, indeed the ratio calculated within the PHSD model is practically constant in the whole range of $\sqrt{s_{NN}}$ considered, but significantly deviates from the ideal-fluid estimate of 0.5. This result is qualitatively consistent with the behavior of these harmonics in Figs. 3 and 6. In contrast, neglecting dynamical quark-gluon degrees of freedom in the HSD model, we obtain a monotonous growth of this ratio.

The dependence of the $v_4/(v_2)^2$ ratio versus the number of participants N_{part} is shown in Fig. 10 for charged particles produced in Au + Au collisions at $\sqrt{s_{NN}} = 200$ GeV. The PHSD results are roughly in agreement

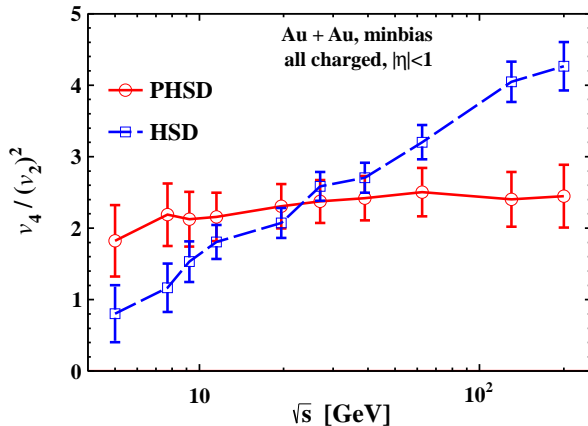


FIG. 9: (Color online) Beam-energy dependence of the ratio $v_4/(v_2)^2$ for Au+Au collisions. The solid and dashed curves are calculated within the PHSD and HSD models, respectively.

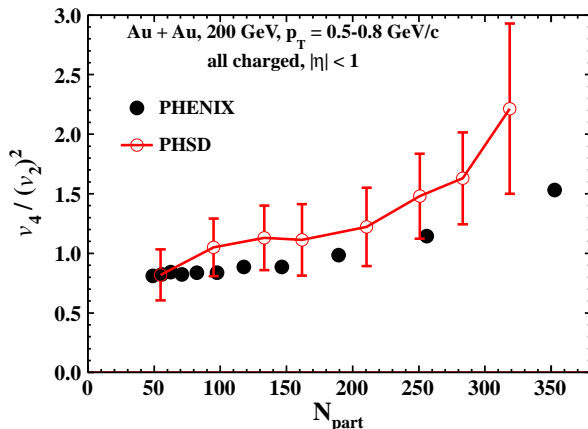


FIG. 10: (Color online) Participant number dependence of the $v_4/(v_2)^2$ ratio of charged particles for Au+Au ($\sqrt{s_{NN}} = 200$ GeV) collisions. The experimental data points for $0.5 < p_T < 0.8$ GeV/c are from Ref. [46].

with the experimental data points from Ref. [59] but overshoot them for $N_{part} \gtrsim 250$. We will come back to this quantity in the last subsection when discussing its p_T dependence.

C. Scaling of flow coefficients

The v_2 coefficient measures the response of the heated and compressed matter to the spatial deformation in the overlap region of colliding nuclei, which is usually quantified by the eccentricity $\epsilon_2 = \langle y^2 - x^2 \rangle / \langle x^2 + y^2 \rangle$. Since the flow response (v_2) is proportional to the driving force (ϵ_2), the ratio v_2/ϵ_2 is used to compare different impact parameters and nuclei.

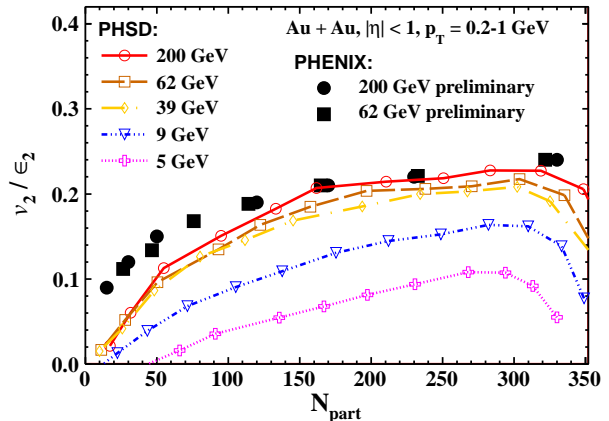


FIG. 11: (Color online) Scaling of v_2/ϵ_2 as a function of the number of participants for different beam energies. Experimental points are for Au + Au collisions at $\sqrt{s_{NN}} = 200$ (circles) and 62 GeV (squares) [60].

In Fig. 11 this ratio is plotted as a function of the participant multiplicity N_{part} . Note that in these calculations the same eccentricity ϵ_2 was used as in the experiment [61]. All PHSD results for $\sqrt{s_{NN}} \gtrsim 40$ GeV are very close to each other and in agreement with experiment. At lower collision energies this scaling starts to be violated with decreasing $\sqrt{s_{NN}}$.

A remarkable property – *universal scaling* – has been proposed in Ref. [62] (see Fig. 12). It appears that v_2/ϵ_2 plotted versus $(1/S)dN_{ch}/dy$ falls on a “universal” curve, which links very different regimes, ranging from Alternating Gradient Synchrotron (AGS) to RHIC energies. Here $S = \pi\sqrt{\langle x^2 \rangle \langle y^2 \rangle}$ is the overlap area of the collision system and dN_{ch}/dy is the rapidity density of charged particles.

As seen in Fig. 12 very different systems vary essentially only in a single scale; this scale does not depend on the collision energy (note that the NA49 data – filled triangles – are beyond this systematics) and is connected to the total entropy produced [64]. Indeed, peripheral and low-energy collisions are likely to produce systems with incomplete thermalization. Since rescattering of the particles is rare in the low-density regime, little change occurs, on average, to the initial momentum distributions. The measured elliptic flow v_2 is therefore proportional to the initial state eccentricity ϵ_2 . This quantity and the space density of the initial particles dN_{ch}/dy are determined via Glauber calculations. In our case we calculate these quantities directly within the PHSD model. Thus,

$$v_2 \propto \frac{1}{S} \frac{dN_{ch}}{dy} \epsilon_2. \quad (5)$$

We point out that only when event-by-event fluctuations in eccentricity are taken into account the universal scaling is observed in PHSD. The term $(1/S)(dN_{ch}/dy)$ contains information about both the longitudinal structure

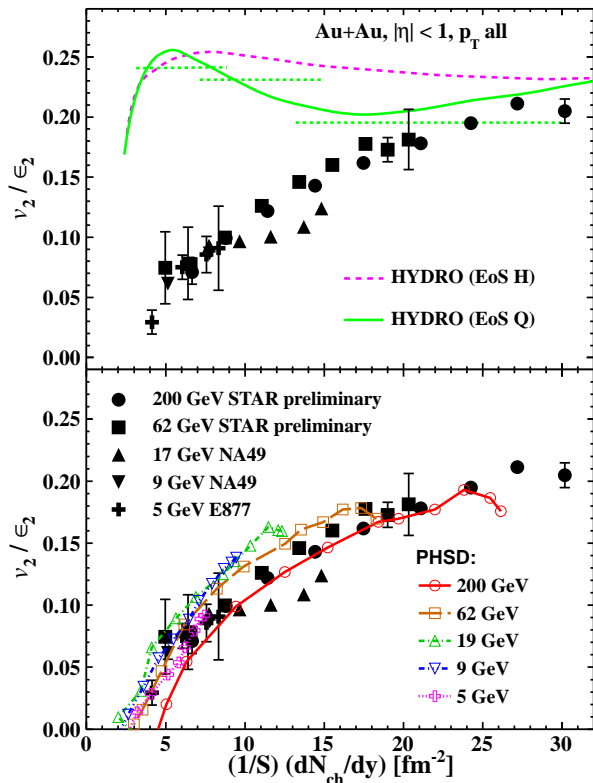


FIG. 12: (Color online) Scaling of v_2/ϵ_2 vs $(1/S)(dN_{ch}/dy)$. The PHSD results are given by lines with open symbols. Predictions of ideal boost-invariant hydrodynamics are shown in the top panel (from Ref. [63]) and explained in the text. Our PHSD results are presented in the bottom panel. The experimental data points for Au+Au collisions at 200 GeV (circles) and 62 GeV (squares) are from Refs. [60, 63].

at freeze-out and the final particle number density (which is a function of the initial temperature T and baryon chemical potential μ_B in the hydro limit).

We therefore use dN_{ch}/dy or, equivalently, the initial entropy density s_0 in central Au+Au collisions as a proxy for the collision energy: At any given collision energy, a measurement of dN_{ch}/dy in the most central collision events fixes the value of s_0 to be used in ideal fluid simulations at that energy. Assuming linear longitudinal expansion without transverse flow at very early time τ_0 , the quantities dN_{ch}/dy and s_0 are thus related by

$$\frac{dN_{ch}}{dy} \propto \tau_0 s_0. \quad (6)$$

In an ideal (isentropic) expansion, the final entropy is equal to the initial entropy content of the system [\sim the initial particle density $n(T, \mu_B)$]. Thus, the systems from AGS to RHIC appear to be controlled by a common scale, related to the total multiplicity, which varies smoothly and drives both v_2/ϵ_2 and $(1/S)(dN/dy)$. This conclusion is a strong indication that microscopic properties of the system (equation of state and mean free path) are

basically unchanged, up to a shift related to this scale, in the experimentally addressed energy range.

In the hydrodynamic limit – implying complete thermalization of the system – the ratio of elliptic flow to eccentricity is saturated at very low impact parameter. In this regime the centrality dependence of the elliptic flow is mainly determined by the initial elliptic anisotropy of the overlap zone in the transverse plane, and the ratio of these two should be approximately constant. This is seen in Fig. 12 where this correlation is plotted by three horizontal lines for three different beam energies according to Ref. [65].

Predictions of ideal boost-invariant hydrodynamics based on calculations of Ref. [65] are also presented in Fig. 12 (top panel). The lines shown are hydrodynamic results for two boost-invariant lattice-inspired equations of state (with a quark-hadron phase transition, marked as “Q”, and for a pure hadronic system “H”) calculated for the fixed impact parameter ($b = 7$ fm) and different particle densities. Note that hydrodynamic results do not scale perfectly in this case and in general exhibit a somewhat flatter centrality dependence at each collision energy. The deviation from experiment is very large for peripheral collisions [$(1/S)dN_{ch}/dy \lesssim 15$], where the application of hydrodynamics is questionable since the mean free path of the degrees of freedom is no longer small compared to the transverse size of the system.

The universal scaling has been investigated in more elaborated dissipative hydrodynamic models in Refs. [66, 67]. A finite shear viscosity η strongly suppresses the buildup of momentum anisotropy and elliptic flow, especially for low multiplicity densities. The viscosity effect changes the slope of the multiplicity scaling for v_2/ϵ_2 but preserves, to a good approximation, its general scaling with $(1/S)dN_{ch}/dy$. However, contrary to experiments, in hydrodynamic simulations – irrespective of fluid viscosity – the elliptic flow does not follow the universal scaling. In principle, the shear viscosity scaled with the entropy density η/s can be extracted in such an analysis; however, the present accuracy of the extracted values is not high enough.

Thus, the experimentally observed scaling in Fig. 12 puts very strong constraints on the initial microscopic properties (entropy density, mean free path, *etc.*), as well as the global longitudinal structure [68].

D. Scaling in pseudorapidity

Another interesting insight on scale invariance in experimental observables is the *longitudinal scaling* seen experimentally. The multiplicity longitudinal scaling, $dN_{ch}/d\eta$, is found for a variety of colliding systems and is often denoted as “limiting fragmentation”. Proposed more than 40 years ago by Feynman [69] and Hagedorn [70], this hypothesis implies that the multiplicity distribution of particles becomes independent of \sqrt{s} for $\sqrt{s} \rightarrow \infty$. From the microscopic point of view the mul-

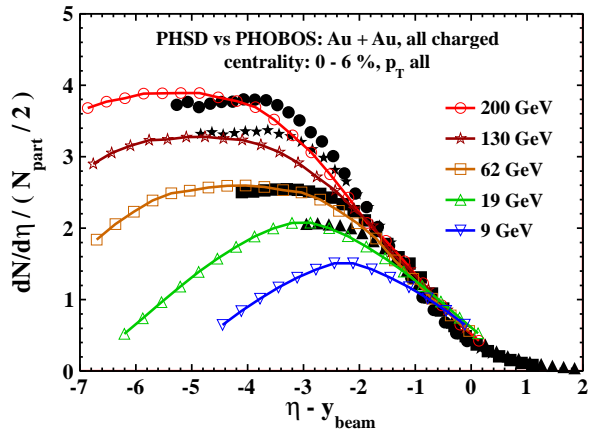


FIG. 13: (Color online) The dependence of the charged particle multiplicity on the shifted pseudorapidity. Experimental data points are from Ref. [71].

tiplicity longitudinal scaling can be understood if the rapidity distributions of produced hadrons are functions of the fraction of the hadron longitudinal momentum $x = 2p_T/\sqrt{s}$ alone but not of the total energy. This picture is very close to the Bjorken scaling of parton distributions. It was found that models combining ideal hydrodynamics and hadronic cascades reproduce the longitudinal multiplicity scaling pretty well, being rather insensitive to the “phase” of the system at thermalization. This is illustrated in Fig. 13 for very central Au+Au collisions within the PHSD model. The limiting fragmentation region is nicely reproduced for $(\eta - y_{beam}) \gtrsim -2$, while some deviations are seen closer to midrapidity for higher collision energies. The situation is different for the elliptic flow, since, unlike $dN_{ch}/d\eta$, the collective flow v_2 is sensitive to the phase of the system as shown before.

As follows from Fig. 14 the PHSD model reproduces the longitudinal v_2 scaling up to comparatively low collision energies (not yet measured). Hadronic results obtained within in the UrQMD model presented in Ref. [73] are quite close to our findings, to be formulated as “a qualitative agreement with experiment”. Such a scaling was observed also for partonic models such as the AMPT and AMPT-SM [73].

We mention that the v_2 scaling with shifted pseudorapidity can be obtained also by solving the Boltzmann equation with an ellipsoidal profile in the initial transverse density [74],

$$\frac{v_2}{\varepsilon} \sim \frac{\langle \sigma v \rangle}{S} \frac{dN_{ch}}{dy}, \quad (7)$$

where σ is the interaction cross section. In line with Eq. (5) in the discussion of the universal scaling, such an ansatz will naturally lead to an observed-like scaling provided that $\langle \sigma v \rangle$ does not vary with rapidity.

Furthermore, a comprehensive analysis of the longitudinal scaling has been performed in Ref. [75] within

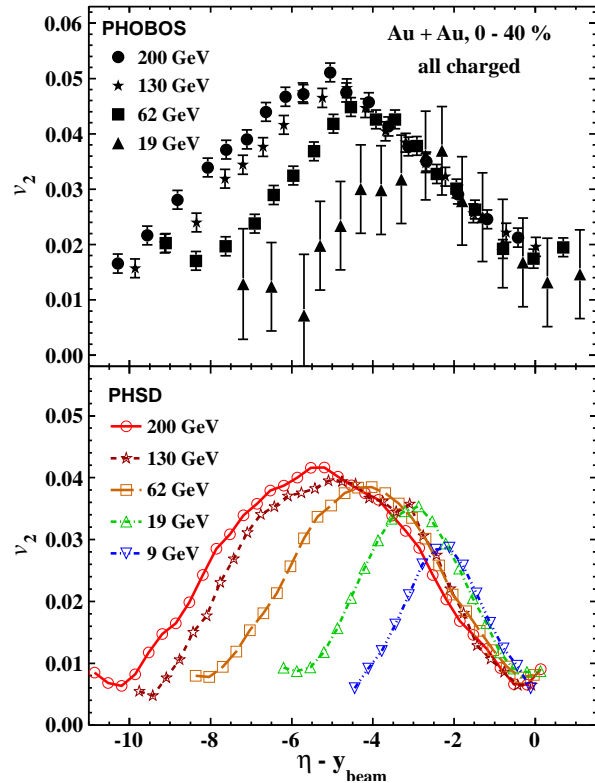


FIG. 14: (Color online) The v_2 dependence versus pseudorapidity as calculated in the PHSD model. The compilation of experimental data points is from Ref. [72].

simple phenomenological models, trying various assumptions for hydrodynamic and kinetic descriptions. The authors conclude that the experimentally observed scaling of *multiplicity* with rapidity and collision energy follows from reasonable models of partonic dynamics. Neither the free-streaming limit nor the ideal-fluid limit are expected to break up this multiplicity scaling [75]. The situation is, however, different with the scaling observed for the elliptic flow v_2 . It is not clear how this scaling could arise within nonideal hydrodynamics, even if its initial conditions mirror closely the ones that reproduce the scaling observed in $dN_{ch}/d\eta$. These remarks address the shape of the scaling distribution. A more serious problem is the absolute value of v_2 . In terms of Eq. (7), to get a reasonable magnitude of v_2 , the cross section σ should be increased to the point where the Knudsen number is well below unity [75]. As demonstrated above, the PHSD model allows us to get reasonable results for the multiplicity and v_2 longitudinal scaling by default without any tuning of parameters.

E. Differential distributions

It was shown in the RHIC experiments that, for a given centrality, the differential elliptic flow for all ob-

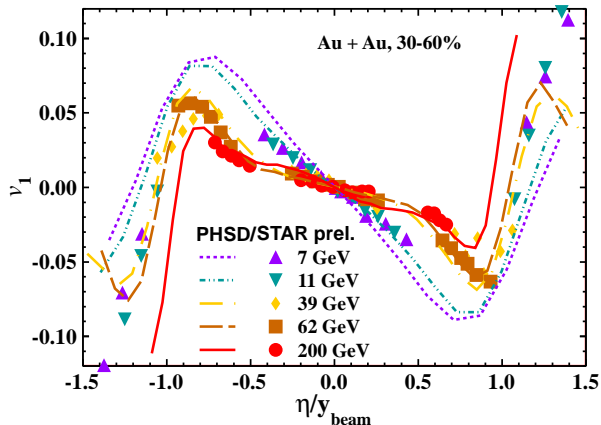


FIG. 15: (Color online) Normalized pseudo-rapidity distributions of the directed flow v_1 in the transient collision energy range. The experimental data points are from the STAR Collaboration [78].

served hadrons scales to a single curve when plotted as v_2/n_q versus E_{TK}/n_q , where n_q is the number of constituent quarks in a given hadron species and E_{TK} is the transverse kinetic energy for these hadrons [76, 77]. This quark number scaling is consistent with the recombination model, which assumes the collective flow to develop on the quark level in the QGP phase. Such a scaling of the elliptic flow v_2 for identified hadrons has been measured by the STAR and PHENIX Collaborations at different centralities for top RHIC energies and recently also within the BES program [28]. Our paper deals only with charged-particle observables and therefore the number of constituent quarks n_q is not accurately defined. The analysis of scaling properties of identified hadrons we postpone to a future study.

We start with the consideration of rapidity distributions $dv_1/d\eta$ of the directed flow [78] and its beam energy dependence as presented in Fig. 15. The directed flow v_1 is the first harmonic coefficient of the above Fourier expansion of the final momentum-space azimuthal anisotropy Eq. (4), and it reflects the collective sideways motion or “bounce-off” of the particles in the final state. Being generated essentially during the nuclear passage time $\sim 2R/\gamma$, the directed flow probes the very early stage of the collision dynamics. In the region closer to the beam/target rapidity than to midrapidity, the directed flow is generated very early even at a pre-equilibrium stage of the collision [79] and thus it probes the onset of bulk collective behavior. In Fig. 15 the directed flow of charged particles is plotted versus the normalized pseudorapidity η/y_{beam} in the large range of the BES collision energies for centrality 30%-60%. We observe that $v_1(\eta/y_{beam})$ shows a beam-energy scaling behavior, though not perfect. Both hydrodynamic and nuclear transport models indicate that the directed flow is a sensitive signature for a possible phase transition,

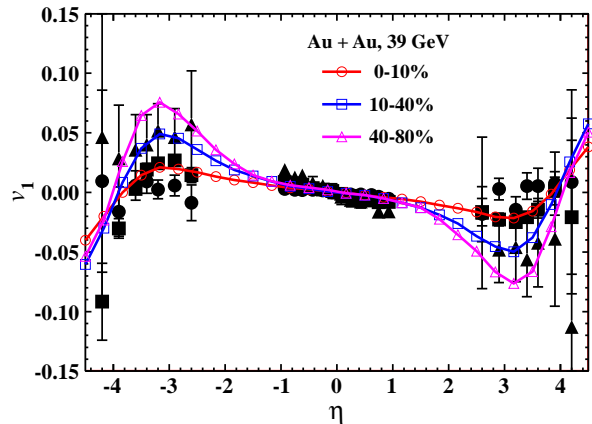


FIG. 16: (Color online) Directed flow distributions at different centralities for Au + Au collisions at $\sqrt{s_{NN}} = 39$ GeV. The experimental data points are from Refs. [78, 83].

especially in the central region of beam-energies under investigation. In particular, the shape of $v_1(y)$ in the midrapidity region is of special interest because it has been argued that differential directed flow may exhibit flatness at midrapidity due to a strong, tilted expansion of the source. Such tilted expansion gives rise to anti-flow [80]. The antiflow is in the opposite direction to the repulsive bounce-off motion of nucleons. If the tilted expansion is strong enough, it can cancel and even reverse the motion in the bounce-off direction and result in a negative $v_1(y)$ slope at midrapidity, potentially producing a wiggle-like structure in $v_1(y)$. A wiggle for baryons is a possible signature of a phase transition between hadronic matter and quark gluon plasma (QGP), although a QGP is not the only possible explanation [80–82]. As seen from Fig. 15 the slope of the $v_1(\eta/y_{beam})$ distribution at $\eta = 0$ is negative and stays almost constant for $\sqrt{s_{NN}} \gtrsim 10$ GeV; its magnitude slightly increases with decreasing beam energy, however, exhibiting no irregularities.

The slope of the pseudorapidity distributions is slightly changed when different criteria for centrality selection are applied as demonstrated in Fig. 16. The influence of this selection is very moderate at midrapidity but becomes noticeably stronger in the target-projectile fragmentation region with increasing impact parameter.

Let us continue with differential distributions of the elliptic flow v_2 by comparing the p_T dependence from data with those from the PHSD model. The results from PHSD for $v_2(p_T)$ are displayed in Fig. 17 for $\sqrt{s_{NN}}$ from 5 to 200 GeV. Also shown are the corresponding results from the STAR Collaboration at $\sqrt{s_{NN}} = 9, 62,$ and 200 GeV (by symbols). The data from PHENIX and STAR at midrapidity indicate that the magnitudes and trends of the differential elliptic flow [$v_2(p_T)$, centrality dependence], are changed only very little over the collision energy range $\sqrt{s_{NN}} = 62 - 200$ GeV, indicating an approximate saturation of the excitation function for

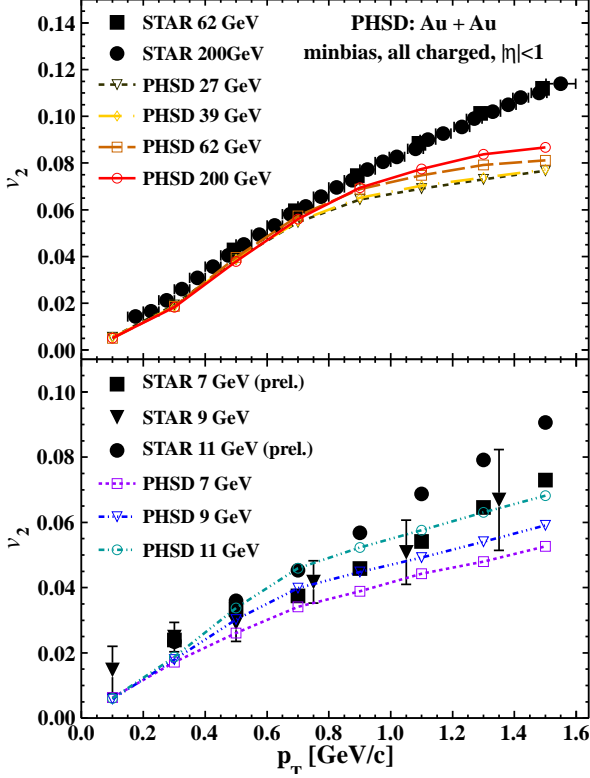


FIG. 17: (Color online) Beam-energy evolution of transverse momentum distributions of $v_2(p_T)$ for Au+Au collisions in comparison to the data of the STAR Collaboration from Refs. [47, 78, 84].

v_2 at these energies [27] as exemplified in Fig. 17. We mention that the PHSD results underestimate the data systematically for $p_T > 1$ GeV, which is attributed to an overestimation of scattering of partons with high transverse momenta. However, the collective flow v_2 of the “bulk matter” is rather well described at all energies without any tuning of parameters.

The momentum distribution of the flow v_3 is also in a quite reasonable agreement with experiment (see Fig. 18).

As pointed out before, the ratios of flow coefficients might shed valuable light on the actual dynamics, since especially the ratio $v_4/(v_2)^2$ is sensitive to the microscopic dynamics. In this respect we show the transverse momentum dependence of the ratio $v_4/(v_2)^2$ in Fig. 19 for charged particles produced in Au+Au collisions at $\sqrt{s_{NN}} = 200$ GeV (20-30% centrality). The PHSD results are quite close to the experimental data points from Ref. [59]; however, they overestimate the measurements by up to 20%. The hydrodynamic results – plotted in the same figure – significantly underestimate the experimental data and noticeably depend on viscosity. The partonic AMPT model [86] discussed above also predicts a slightly lower ratio than the measured one; however, it is in agreement with both hydrodynamic models for $p_T \lesssim$

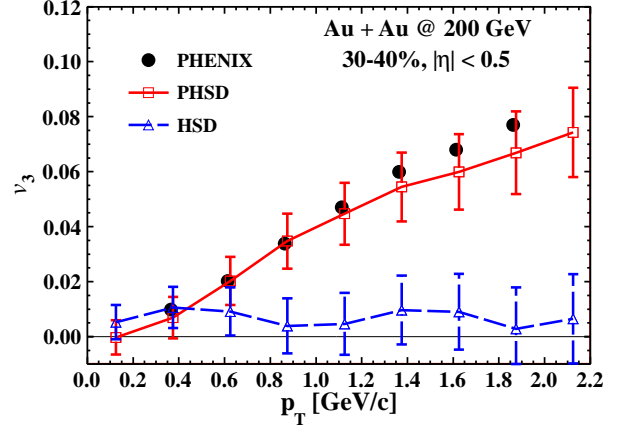


FIG. 18: (Color online) Triangular flow v_3 as a function of transverse momentum p_T for Au + Au collision at $\sqrt{s_{NN}} = 200$ GeV. The data points are from Ref. [52].

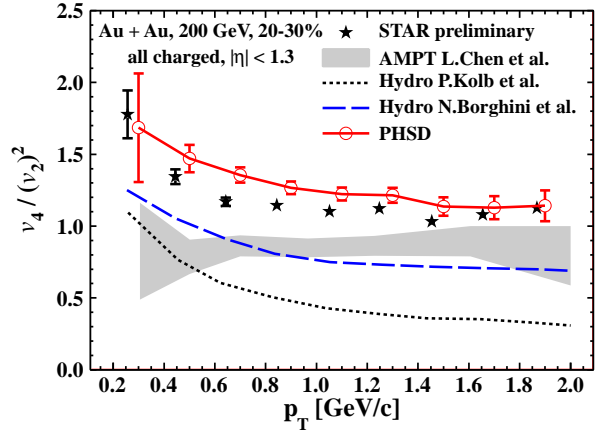


FIG. 19: (Color online) Transverse momentum dependence of the ratio $v_4/(v_2)^2$ of charged particles for Au+Au (at $\sqrt{s_{NN}} = 200$ GeV) collisions. The dashed and dot-dashed lines are calculated within the hydrodynamic approaches from Refs. [58] and [85], respectively. The shaded region corresponds to the results from the AMPT model [86]. The experimental data points are from the STAR Collaboration [59].

0.8 GeV/c. Our interpretation of Fig. 19 is as follows: the data are not compatible with ideal hydrodynamics and a finite shear viscosity is mandatory (in viscous hydrodynamics) to come closer to the experimental observations. The kinetic approaches AMPT and PHSD perform better but either overestimate (in AMPT) or slightly underestimate (in PHSD) the scattering rate of soft particles. An explicit study of the centrality dependence of these ratios should provide further valuable information.

IV. CONCLUSIONS

In summary, relativistic collisions of Au+Au from $\sqrt{s_{NN}} = 5$ to 200 GeV have been studied within the PHSD approach, which includes the dynamics of explicit partonic degrees of freedom as well as dynamical local transition rates from partons to hadrons and also the final hadronic scatterings. Whereas earlier studies have been carried out for longitudinal rapidity distributions of various hadrons, their transverse mass spectra, and the elliptic flow v_2 as compared to available data at SPS and RHIC energies [32, 33], here we have focused on the PHSD results for the collective flow coefficients v_1 , v_2 , v_3 , and v_4 in comparison to recent experimental data in the large energy range from the RHIC Beam Energy Scan (BES) program, as well as different theoretical approaches ranging from hadronic transport models to ideal and viscous hydrodynamics. We mention explicitly that the PHSD model from Ref. [33] has been used for all calculations performed in this study and no tuning (or change) of model parameters has been performed.

We have found that the anisotropic flows – elliptic v_2 , triangular v_3 , and hexadecapole v_4 – are reasonably described within the PHSD model in the whole transient energy range, naturally connecting the hadronic processes at lower energies with ultrarelativistic collisions where the quark-gluon degrees of freedom become dominant. The smooth growth of the elliptic flow v_2 with the collision energy demonstrates the increasing importance of partonic degrees of freedom. This feature is reproduced by neither hadron-string based kinetic models nor a multi phase transport (AMPT) model treating the partonic phase in a simplified manner. Other signatures of the transverse collective flow, the higher-order harmonics of the transverse anisotropy v_3 and v_4 , change only weakly from $\sqrt{s_{NN}} \sim 7$ GeV to the top RHIC energy of $\sqrt{s_{NN}} = 200$ GeV, roughly in agreement with experiment. As shown in this study, this success is related to a consistent treatment of the interacting partonic phase in PHSD, whose fraction increases with the collision energy.

The observables calculated within the PHSD model exhibit some scaling properties for collision energies above $\sqrt{s_{NN}} = 40$ GeV. In particular, the universal scaling of v_2/ϵ_2 versus $(1/S)dN_{ch}/dy$ (*cf.* Fig. 12) is approximately reproduced as well as the longitudinal scaling of the charged particle pseudorapidity distributions of the elliptic flow v_2 in $(\eta - y_{beam})$ representation (*cf.* Figs. 13 and 14) in this energy range. This feature is not reproduced by hadronic transport models (such as HSD and UrQMD) and meets (severe) problems in the various hydrodynamic descriptions.

The analysis of correlations between particles emitted in ultrarelativistic heavy-ion collisions at large relative rapidity has revealed an azimuthal structure that can be interpreted as being solely due to collective flow [87, 88]. This interesting new phenomenon, denoted as triangu-

lar flow, results from initial-state fluctuations and a subsequent hydrodynamic-like evolution. Unlike the usual directed flow, this phenomenon has no correlation with the reaction plane and should depend weakly on rapidity. Event-by-event hydrodynamics [89] has been a natural framework for studying this triangular collective flow but it has been of interest also to investigate these correlations in terms of the PHSD model. We have found the third harmonics to increase steadily in PHSD with bombarding energy. The coefficient v_3 is compatible with zero for $\sqrt{s_{NN}} > 20$ GeV in case of the hadronic transport model HSD, which does not develop “ridge-like” correlations. In this energy range PHSD gives a positive v_3 due to dominant partonic interactions.

Different harmonics can be related to each other and, in particular, hydrodynamics predicts that $v_4 \propto (v_2)^2$ [58]. In this work it was noted also that v_4 is largely generated by an intrinsic elliptic flow (at least at high p_T) rather than the fourth-order moment of the fluid flow. Indeed, the ratio $v_4/(v_2)^2$ calculated within the PHSD model is approximately constant in the whole considered range of $\sqrt{s_{NN}}$ but significantly deviates from the ideal fluid estimate of 0.5. In contrast, neglecting dynamical quark-gluon degrees of freedom in the HSD model, we obtain a monotonous growth of this ratio.

The transverse momentum dependence of the ratio $v_4/(v_2)^2$ at the top RHIC energy has given further interesting information (*cf.* Fig. 19) by comparing the various model results to the data from STAR, which are interpreted as follows: the STAR data are not compatible with ideal hydrodynamics and a finite shear viscosity is mandatory (in viscous hydrodynamics) to come closer to the experimental ratio observed. The kinetic approaches AMPT and PHSD perform better but either overestimate (in AMPT) or slightly underestimate the scattering rate of soft particles (in PHSD). An explicit study of the centrality dependence of these ratios should provide further valuable information.

It will be promising to extend our studies to asymmetric heavy-ion collisions that can be used to constrain models dealing with flow fluctuations in heavy-ion collisions but with a larger sensitivity for v_2 -related observables than for v_3 [90]. Independently, an extension of the PHSD approach to LHC energies with possible color-glass-condensate initial conditions has to be performed in future.

Acknowledgements

We are thankful to O. Linnyk and G. Torrieri for helpful discussions. This work was supported in part by the DFG Grants No. WA 431/8-1 and No. CA 124/7-1, the RFFI Grants No. 08-02-01003-a, the Ukrainian-RFFI Grant No. 09-02-90423-ukr-f-a, and the LOEWE center HIC for FAIR.

-
- [1] J.-Y. Ollitrault, Phys. Rev. **D46**, 229 (1992).
- [2] U. Heinz and P. Kolb, Nucl. Phys. **A702**, 269 (2002).
- [3] E. Shuryak, Prog. Part. Nucl. Phys. **62**, 48 (2009).
- [4] E.V. Shuryak, Nucl. Phys. **A750**, 64 (2005).
- [5] M. Gyulassy and L. McLerran, Nucl. Phys. **A750**, 30 (2005).
- [6] A. Peshier and W. Cassing, Phys. Rev. Lett. **94**, 172301 (2005).
- [7] Y. Aoki *et al.*, Nature **443**, 675 (2006).
- [8] M. Cheng *et al.*, Phys. Rev. **D77**, 014511 (2008).
- [9] Y. Aoki *et al.*, JHEP **0906**, 088 (2009); S. Borsanyi *et al.*, JHEP **1009**, 073 (2010); JHEP **1011**, 077 (2010).
- [10] A. Adare *et al.* (for the PHENIX Collaboration), Phys. Rev. Lett. **98**, 172301 (2007).
- [11] P. Romatschke and U. Romatschke, Phys. Rev. Lett. **99**, 172301 (2007).
- [12] Z. Xu, C. Greiner and H. Stöcker, Phys. Rev. Lett. **101**, 082302 (2008).
- [13] R.A. Lacey *et al.*, Phys. Rev. Lett. **98**, (2007) 092301.
- [14] H.-J. Drescher, A. Dumitru, C. Gombeaud and J.-Y. Ollitrault, Phys. Rev. **C76**, 024905 (2007).
- [15] A.K. Chaudhuri, Phys. Rev. **C81**, 044905 (2010).
- [16] N. Borghini and J.-Y. Ollitrault, Phys. Lett. **B642**, 227 (2006).
- [17] R.S. Bhalerao *et al.*, Phys. Lett. **B627**, 49 (2005).
- [18] M. Miller and R. Snellings, nucl-ex/0312008 (2003); Y. Hama *et al.*, Phys. Atom. Nucl. **71**, 1558 (2008); B. Alver *et al.*, Phys. Rev. Lett. **98**, 242302 (2007).
- [19] A.P. Mishra, R.K. Mohapatra, P.S. Saumia, A.M. Srivastava, Phys. Rev. **C77**, 064902 (2008).
- [20] B. Alver and G. Roland, Phys. Rev. **C81**, 054905 (2010); [Erratum-ibid. **C82**, 039903 (2010)].
- [21] J. Xu, Ch.M. Ko, Phys. Rev. **C83**, 021903 (2011).
- [22] H. Petersen, M. Bleicher, Phys. Rev. **C81**, 044906 (2010); H. Petersen, G.-Y. Qin, S. A. Bass, B. Müller, Phys. Rev. **C82**, 041901 (2010); G.-Y. Qin, H. Petersen, S. A. Bass, B. Müller, Phys. Rev. **C82**, 064903 (2010).
- [23] J. Adams *et al.* (the STAR Collaboration), Phys. Rev. Lett. **95**, 152301 (2005); F. Wang (for the STAR Collaboration), J. Phys. **G30**, S1299 (2004); J. Adams *et al.* (for the STAR Collaboration), Phys. Rev. **C73**, 064907 (2006); J. Putschke, J. Phys. **G34**, S679 (2007); J. Adams *et al.* (for the Star Collaboration), Phys. Rev. **C75**, 034901 (2007); A. Adare *et al.* (for the PHENIX Collaboration), Phys. Rev. **C78**, 014901 (2008); B. Alver *et al.* (for the PHOBOS Collaboration), J. Phys. **G35**, 104080 (2008).
- [24] S.A. Voloshin, Nucl. Phys. **A749**, 287 (2005).
- [25] H. Petersen, V. Bhattacharya and S.A. Bass, C. Greiner, Phys. Rev. **C84**, 054908 (2011).
- [26] K. Aamodt *et al.* (for the ALICE Collaboration), Phys. Rev. Lett. **105**, 252302 (2010).
- [27] A. Taranenko (for the PHENIX Collaboration), arXiv:1101.5069.
- [28] G. Odyniec, Acta Phys. Polon. **B40**, 1237 (2009); B.I. Abelev *et al.* (for the STAR Collaboration), Phys. Rev. **C81**, 024911 (2010).
- [29] M.M. Aggarwal *et al.* (for the STAR Collaboration), arXiv:1007.2613.
- [30] M. Nasim, L. Kumar, P.K. Netrakanti and B. Mohanty, Phys. Rev. **C82**, 054908 (2010).
- [31] V.P. Konchakovski, E.L. Bratkovskaya, W. Cassing, V.D. Toneev and V. Voronyuk, Phys. Rev. **C85**, 011902 (2012).
- [32] W. Cassing and E.L. Bratkovskaya, Nucl. Phys. **A831**, 215 (2009).
- [33] E.L. Bratkovskaya, W. Cassing, V.P. Konchakovski and O. Linnyk, Nucl. Phys. **A856**, 162 (2011).
- [34] W. Cassing, Nucl. Phys. **A 791**, 365 (2007).
- [35] W. Cassing, Nucl. Phys. **A 795**, 70 (2007).
- [36] W. Ehehalt and W. Cassing, Nucl. Phys. **A 602**, 449 (1996).
- [37] W. Cassing and E.L. Bratkovskaya, Phys. Rep. **308**, 65 (1999).
- [38] H.-U. Bengtsson and T. Sjöstrand, Comp. Phys. Commun. **46**, 43 (1987).
- [39] K.H. Ackermann *et al.* (for the STAR Collaboration), Phys. Rev. Lett. **86**, 402 (2001).
- [40] S.A. Bass *et al.*, Prog. Part. Nucl. Phys. **41**, 255 (1998); M. Bleicher *et al.*, J. Phys. **G25**, 1859 (1999).
- [41] E.L. Bratkovskaya, W. Cassing, and H. Stöcker, Phys. Rev. **C67**, 054905 (2003).
- [42] W. Cassing, Eur. Phys. J. ST **168**, 3 (2009).
- [43] H. Weber, E.L. Bratkovskaya, W. Cassing, H. Stocker, Phys. Rev. **C67**, 014904 (2003).
- [44] E. L. Bratkovskaya, *et al.*, Phys. Rev. **C69**, 054907 (2004); Phys. Rev. Lett., **92**, 032302 (2004).
- [45] Z.W. Lin, C.M. Ko, Phys. Rev. **C65**, 034904 (2002); Z.W. Lin, C.M. Ko, B.A. Li, B. Zhang, S. Pal, Phys. Rev. **C72**, 064901 (2005).
- [46] X. -Y. Gong (PHENIX Collaboration), J. Phys. G **38**, 124146 (2011).
- [47] B.I. Abelev *et al.* (for the STAR Collaboration), Phys. Rev. **C81**, 024911 (2010).
- [48] W. Cassing and E.L. Bratkovskaya, Phys. Rev. **C78**, 034919 (2008).
- [49] S. Mattiello and W. Cassing, Eur. Phys. J. **C70**, 243 (2010).
- [50] N. Demir and S. A. Bass, Phys. Rev. Lett. **102**, 172302 (2009).
- [51] H. Petersen, C. Coleman-Smith, S. A. Bass, and R. Wolpert, J. Phys. **G38**, 045102 (2011).
- [52] A. Adare *et al.* (for the PHENIX Collaboration), Phys. Rev. Lett. **107**, 252301 (2011).
- [53] A.M. Poskanzer and S.A. Voloshin, Phys. Rev. **C58**, 1671 (1998).
- [54] A. Bilandzic, R. Snellings and S. Voloshin, Phys. Rev. **C83**, 044913 (2011).
- [55] B.B. Back *et al.*, (for the PHOBOS Collaboration), Phys. Rev. **C72**, 051901 (2005).
- [56] J. Xu and C.M. Ko, Phys. Rev. **C84**, 014903 (2011).
- [57] B. Schenke, S. Jeon, and C. Gale, Phys. Rev. Lett. **106**, 042301 (2011).
- [58] P.F. Kolb, Phys. Rev. **C68**, 031902(R) (2003).
- [59] Y. Bai (for the STAR Collaboration), J. Phys. **G34**, S903 (2007).
- [60] M. Shimomura (for the PHENIX Collaboration), PoS **WPCF2011**, 070 (2011).
- [61] A. Adare *et al.*, (for the PHENIX Collaboration), Phys. Rev. Lett. **105**, 062301 (2010).
- [62] S.A. Voloshin and A.M. Poskanzer, Phys. Lett. **B474**, 27 (2000).

- [63] S. A. Voloshin, J. Phys. **G34**, S883 (2007).
- [64] H. Caines, Eur. Phys. J. **C49**, 297 (2007).
- [65] P.F. Kolb, J. Sollfrank and U. Heinz, Phys. Rev. **C62** 054909 (2000).
- [66] H. Song, U.W. Heinz, Phys. Rev. **C78**, 024902 (2008).
- [67] A. K. Chaudhuri, Nucl. Phys. A **862**, 180 (2011); Phys. Rev. **C82**, 047901 (2010); Nucl. Phys. **A862**, 180 (2011).
- [68] G. Torrieri, Phys. Rev. **C76**, 024903 (2007).
- [69] R.P. Feynman, Phys. Rev. Lett. **23**, 1415 (1969).
- [70] R. Hagedorn, Nucl. Phys. **B24**, 93 (1970).
- [71] B.B. Back *et al.* (for the PHOBOS Collaboration), Phys. Rev. **C74**, 021901 (2006).
- [72] W. Busza (for the PHOBOS Collaboration), Nucl. Phys. **A830**, 35c (2009).
- [73] M. Nasim, C. Jena, L. Kumar, P.K. Netrakanti, and B. Mohanty, Phys. Rev. **C83**, 054902 (2011).
- [74] H. Heiselberg and A.M. Levy, Phys. Rev. **C59**, 2716 (1999).
- [75] G. Torrieri, Phys. Rev. **C82**, 054906 (2010).
- [76] R.A. Lacey and A. Taranenko, **PoS C FRNC2006** (2006) 021.
- [77] A. Adare *et al.*, (for the PHENIX Collaboration), Phys. Rev. Lett. **98**, 162301 (2007).
- [78] Y. Pandit (for the STAR Collaboration), J. Phys. Conf. Ser. **316**, 012001 (2011).
- [79] H. Sorge, Phys. Rev. Lett. **78**, 2309 (1997).
- [80] L.P. Csernai and D. Rohrlich, Phys. Lett. **B458**, 454 (1999).
- [81] J. Brachmann *et al.*, Phys. Rev. **C61**, 024909 (2000).
- [82] H. Stoecker, Nucl. Phys. **A750**, 121 (2005).
- [83] B.I. Abelev *et al.* (for the STAR Collaboration), Phys. Rev. Lett. **101**, 252301 (2008).
- [84] B.I. Abelev *et al.* (for the STAR Collaboration), Phys. Rev. **C75**, 054906 (2007); J. Adams *et al.* (for the STAR Collaboration), Phys. Rev. **C72**, 014904 (2005).
- [85] N. Borghini and J.-Y. Ollitrault, Phys. Lett. **B642**, 227 (2006).
- [86] L.W. Chen, C.M. Ko and Z.W. Lin, Phys. Rev. **C69**, 031901 (2004).
- [87] D. Teaney and L. Yan, Phys. Rev. **C83**, 064904 (2011).
- [88] M. Luzum, C. Gombeaud and J.-Y. Ollitrault, Phys. Rev. **C81** 054910 (2010).
- [89] F.G. Gardim, F. Grassi, Y. Hama, M. Luzum and J.-Y. Ollitrault, Phys. Rev. **C83**, 064901 (2011).
- [90] Md. R. Haque, Md. Nasim, B. Mohanty, Phys. Rev. **C84**, 067901 (2011).